

Estimating the uncertainties of satellite derived soil moisture at global scale

François Gibon^{a,*}, Arnaud Mialon^a, Philippe Richaume^a, Nemesio Rodríguez-Fernández^a, Daniel Aberer^b, Alexander Boresch^c, Raffaele Crapolicchio^d, Wouter Dorigo^b, Alexander Gruber^b, Irene Himmelbauer^b, Wolfgang Preimesberger^b, Roberto Sabia^e, Pietro Stradiotti^b, Monika Tercjak^c, Yann H. Kerr^a

^a Centre d'Etudes Spatiales de la Biosphère (CESBIO) Université de Toulouse CNES/CNRS/INRAe/IRD/UPS, 18 Avenue Edouard Belin, Toulouse, France

^b Technische Universität Wien, Department of Geodesy and Geoinformation, Vienna, Austria

^c Angewandte Wissenschaft Software und Technologie (AWST) GmbH, Vienna, Austria

^d Serco SpA for European Space Agency, ESA/ESRIN, Frascati, Italy

^e European Space Agency, ESA/ESRIN, Frascati, Italy

ARTICLE INFO

Keywords:

Soil moisture
Uncertainty
Passive microwave remote sensing
SMOS
ISMN

ABSTRACT

This study attempts to derive the uncertainty of the soil moisture estimation from passive microwave satellite mission at global scale. To do so, the approach is based on the sensitivity of the Soil Moisture and Ocean Salinity (SMOS) soil moisture retrieval quality to the land surface characteristics within its footprint (presence of forest, topography, open water bodies, sand, clay, bulk density and soil organic carbon content). First, we performed a global assessment of SMOS using *in situ* measurements from the International Soil Moisture Network (ISMN) as reference, with more than 1900 ISMN stations and 10 years of SMOS data. This assessment shows that the ubRMSD scores vary greatly between locations (with a mean of $0.074 \text{ m}^3 \text{ m}^{-3}$ and an interquartile range of $0.030 \text{ m}^3 \text{ m}^{-3}$). Second, the scores are analyzed for different surface conditions within the satellite footprint. The best agreement between the ground measurement and SMOS time series are obtained for low forest cover, low topographic complexity, and marginal presence of open water bodies within the SMOS footprint. Soil parameters also have an impact, with better scores for sandier soils with a high bulk-density and low soil organic carbon content. Finally, we propose to extrapolate the obtained relationships, using a multiple linear regression, in order to derive a global map of SMOS uncertainties based on surface conditions. This map of predicted uncertainties show a diverse range of ubRMSD values across the globe (with a mean of $0.076 \text{ m}^3 \text{ m}^{-3}$ and an interquartile range of $0.031 \text{ m}^3 \text{ m}^{-3}$) depending on the surface characteristics. At the ISMN site location, the predicted ubRMSD shows similar results than the comparison between SMOS and the *in situ* measurements. The map of predicted SMOS ubRMSD represents an upper bound estimate of the SMOS uncertainty, as it includes the uncertainties of the *in situ* sensor measurements and the scale mismatch. Further investigations will focus on the different components of this uncertainty budget to obtain a better assessment of the absolute uncertainties of SMOS soil moisture retrievals across the globe.

1. Introduction

The Global Climate Observing System (World Meteorological Organization, United Nations, and International Council for Science) considers soil moisture (SM) as an Essential Climate Variable (ECV) since 2010. It is a key variable driving the water and energy balance at the soil-atmosphere interface (Seneviratne et al., 2010; Koster et al., 2004). Its observation and monitoring are crucial in a number of scientific and application domains such as climate change diagnostic and climatology

(Douveille and Chauvin, 2000), agricultural applications (Bolten et al., 2010; Shin et al., 2006; Gibon et al., 2018) or weather forecast (Muñoz-Sabater et al., 2018; Drusch, 2007), among others.

Among the various methodologies available to estimate soil water content (*in situ* measurements, models), satellite remote sensing observations provide large-scale measurements. The lower frequency part of the microwave domain (400 MHz - 2 GHz) is particularly well adapted to monitor surface soil moisture variability (Schmugge, 1978; Ulaby et al., 1981; Kerr, 2006), which led to the development of different missions at

* Corresponding author.

E-mail address: francois.gibon@univ-tlse3.fr (F. Gibon).

<https://doi.org/10.1016/j.srs.2024.100147>

Received 27 February 2024; Received in revised form 26 June 2024; Accepted 3 July 2024

Available online 9 July 2024

2666-0172/© 2024 The Authors. Published by Elsevier B.V. This is an open access article under the CC BY license (<http://creativecommons.org/licenses/by/4.0/>).

L-band such as Soil Moisture and Ocean Salinity (SMOS) (Kerr et al., 2010) or Soil Moisture Active Passive (SMAP) (Entekhabi et al., 2010).

Climate analysis need data records that are provided with uncertainties (Merchant et al., 2017). It is however challenging to estimate the uncertainty of geophysical variables such as SM, derived from satellite sensors. This is particularly the case for large footprints for which the true reference is unknown. The method usually used to assess the accuracy of remotely sensed soil moisture, consists in comparing the satellite estimates with ground measurements (Gruber et al., 2020a; Loew et al., 2017). The statistics obtained from this comparison represent a diversity of uncertainties originating from different sources that include the satellite sensor, the reference dataset and the spatio-temporal scale mismatch between the reference and the data to be evaluated. Additionally, due to the scarcity and spatial distribution of ground measurements, satellite data are not assessed everywhere.

Numerous studies have already been carried out to assess the quality of the soil moisture estimation derived from satellite mission such as SMOS (Colliander et al., 2023; Al-Yaari et al., 2019; Al Bitar et al., 2012; Albergel et al., 2012). In (Kerr et al., 2016), authors evaluated different versions of SMOS data using *in situ* measurements as a reference, while (Leroux et al., 2013) identified the potential error sources using the triple collocation method. In (Molero et al., 2018), authors investigated the effect of the timescale on the scale mismatch with the reference. These studies show that numerous factors can affect the quality of retrieval, such as the accuracy of the sensor, the simplification of the physics by the algorithm, the Radio Frequency Interferences (RFI), and also the content of the satellite footprint. For example, the presence of vegetation within the footprint can affect the satellite's ability to measure ground emission due to the vegetation water content.

This study aims at deriving the uncertainties of the soil moisture estimation from a passive microwave satellite mission at the global scale. In our case, the SMOS mission is used as an example, but the extrapolation method we use to derive uncertainties at a global scale may be applied to any other satellite-based soil moisture product. The novelty of this approach lies in the use of the relationships between the uncertainty of satellite-derived soil moisture and the composition of the land surface within the satellite's footprint. To do so, the SMOS uncertainty, derived using *in situ* measurements, is extrapolated at global scale using its sensitivity to the land surface condition. We first present the data in Section 2 and method in Section 3, then, in Section 4.1 we present the results of the global assessment of SMOS using the International Soil Moisture Network (ISMN) data as a reference. Then, the validation scores, analyzed regarding the SMOS footprint content in terms of geophysical parameters, are depicted in Section 4.2. A model is presented in Section 4.3 to relate the SMOS uncertainty and the surface condition. Finally, results, caveats, and limitations are discussed in Section 5.

2. Data

To address our objectives, this study considers three SM datasets that are SMOS, ISMN and ERA5 (ECMWF Reanalysis v5). The geophysical footprint content is characterized using land cover from the International Geosphere Biosphere Program (IGBP) database and the soil parameters using the Harmonized World Soil Database (FAO HWSO) and SoilGrids, which are described below.

2.1. Soil moisture datasets

● Satellite retrievals: SMOS Level 2 version 700 soil moisture product

Based on synthetic aperture radiometry at L-band (1.413 GHz), SMOS measures fully polarised Brightness Temperatures (TB) at multiple incidence angles. To retrieve the geophysical parameters such as soil moisture, a Radiative Transfer Model (RTM) is used to simulate the

SMOS incidence angle TB profile (Kerr et al., 2012). The RTM used in this product is the L-band Microwave Emission of the Biosphere (L-MEB) model (Wigneron et al., 2007), which is initialized by auxiliary data that describe as accurately as possible the SMOS footprint content in terms of land cover, soil properties, vegetation properties and temperatures (ground and vegetation). The SMOS TB profile and the simulated TB profile are then compared, and the model is fitted to the SMOS measurements through minimizing a cost function measuring the differences between the two. Two variables are retrieved: the surface Soil Moisture (SM) and the Vegetation Optical Depth (VOD). SMOS soil moisture products are delivered on various grids depending on the processing level. The Level 2 Soil Moisture (L2SM) product, version 700, is projected onto a 15 km resolution grid (Sahr et al., 2003; Talone et al., 2015). For each node, and depending on the incidence angle, the interception of the antenna beam with the Earth surface defines an ellipse with evolving shape characteristics (flatness, surface, axis direction) (Kerr et al., 2012, 2020). For the purpose of this study, we use a Blackman function that approximates the average of the antenna gain pattern (diameter of ~43 km at -3 dB).

● *In situ* measurements: The International Soil Moisture Network (ISMN)

Initiated in 2009, the ISMN (<https://ismn.earth> (Dorigo et al., 2021),) has become the main reference source for any satellite soil moisture mission through stable long term financing, the global collaboration with voluntary data distributors, and more over through the availability of long-term, harmonized, quality controlled and free useable *in situ* soil moisture measurements. The establishment of the ISMN, its development and maintenance are the combined effort of the hosts the German Federal office for Hydrology (BfG), and the International Center for Water Resources and Global change (ICWRGC) with funding from the German Federal Ministry of Transport and Digital Infrastructure (BMDV), as well as through international collaboration with the Vienna University of Technology (TU Wien), the European Space Agency (ESA), the Global Energy and Water Exchange Project (GEWEX), the Committee on Earth Observation Satellites (CEOS), GCOS Terrestrial Observation Panel Climate, the Group on Earth Observation (GEO), the Global Terrestrial Network Hydrology (GTN-H), and the Rutgers University. The ISMN consists of around 80 networks which represent about 3000 stations containing about 5320 time series (=sensors) in the first 10 cm soil depth. We focus on this top soil layer as it is relevant in the context of satellite due to the penetration depth of a satellite soil moisture sensor. The sites are located in various climate environment, but unevenly distributed, as it can be seen in (Dorigo et al., 2021). Furthermore, soil moisture time series are available from 1952 up to near real time (including actively updated and historical datasets) while the set-up, probe technologies and temporal coverage vary per station and sensor due to the voluntary data collection collaborations with the ISMN. For time consistency with the SMOS mission, only data acquired within the time window 2010–2020 are used (data from the ISMN was downloaded on June 2021), and ISMN data are considered as a reference in this study. The spatial locations of the sites and the references to each network used can be found in the list Appendix A.

● Modelled soil moisture: ERA5

ERA5 is the fifth generation of reanalysis of the climate and weather forecast run at ECMWF (European Centre for Medium-Range Weather Forecasts). It is the result of the assimilation of observations into numerical models to provide estimates of land and atmospheric variables from 1940 to present (Hersbach et al., 2018). Among the large numbers of available variables, the product provides hourly soil moisture information (soil layer depth used here: 0–0.07 m) at a global scale at a resolution of $0.25^\circ \times 0.25^\circ$.

2.2. Geophysical footprint content

In this study, the SMOS geophysical footprint content is quantified using the auxiliary database of the SMOS L2v700 (Kerr et al., 2012). The mean antenna pattern (Blackman function) is applied to each SMOS nodes to the 4×4 km auxiliary data in order to compute the surface conditions monitored by the radiometer.

The soil texture (percentage of sand, clay, and bulk density value) is obtained from the Food and Agriculture Organization - Harmonized World Soil Database (FAO HWSD) map which is built through merging more than 16 000 regional and national soil information maps (SOTER, ESD, Soil Map of China, WISE) and the FAO-UNESCO Soil Map of the World at a 30 arc-second (F. G, 2008).

The Soil Organic Carbon content (SOC) is derived from the SoilGrids database, which is a global digital soil mapping that uses over 230 000 soil profile observations from the WoSIS database and a series of environmental covariates. Covariates were selected from a pool of over 400 environmental layers from Earth observation derived products and other environmental information including climate, land cover and terrain morphology (Poggio et al., 2021).

The International Geosphere Biosphere Program (IGBP) database describes the land cover with 17 classes at 1 km resolution. This database is derived from satellite observations such as Advanced Very High Resolution Radiometer (AVHRR) and other remote sensing data sets (Loveland et al., 1999).

3. Method

The method used in this study is summarized in the flowchart presented in Fig. 1.

The SMOS evaluation results using ISMN as a reference is used to set up a multiple linear regression model which relates the SMOS unbiased Root Mean Square Difference (ubRMSD; referring to the standard deviation difference) to the surface conditions in order to derive a map of SMOS uncertainties at global scale. The paper focuses on the ubRMSD as the purpose of this study is to assess the uncertainties of the derived SM (Gruber et al., 2020b).

The first step of the flowchart described in Fig. 1 is to assess the SMOS data using ISMN ground measurements. To do so, the data are processed following the validation chain in Fig. 2.

The spatial collocation between the probe location and the SMOS node is performed using the nearest neighbor method. Then, the soil moisture time series from the two datasets are filtered ("Filtering" step in Fig. 2). SMOS dataset are filtered considering three information that are present in the product. First, the field "CHI2" is checked. This field is a quality indicator of the retrieval, and values $\chi^2 \geq 0.05$ mean the SM retrieval is good. Second, poor quality SM due to RFI contamination are detected with the fields "RFIP", which stands for the probability that brightness temperatures are affected by an RFI. A threshold of 0.1 is used to consider that the retrieval can not be achieved correctly. Finally, a last

filter is based on the complexity of the topography. The flag "FLTOPO" is used, and retrieval SM with FLTOPO equal to 0 are kept. This flag is set to 1 if the SMOS footprint is too complex in terms of topography that no model can account for this effect. The ISMN dataset filtering strategy considered the following criteria. We only kept probes close to the near surface (depth ≤ 10 cm) and measurements with the quality flag "G" (Good = passing all automatic quality checks from the ISMN) which we set to 1.

The two filtered datasets are collocated time wise based on the nearest *in situ* measurement within the limit of $|\Delta t| \leq 30$ min of each SMOS observation. Finally, the agreement between the two datasets (of N samples) θ^{SMOS} and θ^{ref} is quantified using ubRMSD:

$$ubRMSD = \sqrt{\frac{1}{N} \sum_{i=1}^N [(\theta_i^{SMOS} - \bar{\theta}^{SMOS}) - (\theta_i^{ref} - \bar{\theta}^{ref})]^2} \quad (1)$$

with i the N th collocated sample of the soil moisture time series θ^{SMOS} and θ^{ref} , $\bar{\theta}$ stands for the respective time series average.

Once the ubRMSD is processed for in total 1991 filtered *in situ* time series, its sensitivity to the surface conditions is analyzed. To do so, linear regressions are established between the ubRMSD and different surface conditions of the SMOS footprint content. An approach based on multiple linear regression further specifies the dependency of uncertainties with surface conditions (with intercept and linear term for each descriptor). Finally, the multiple linear regression is extended to SMOS nodes without *in situ* sites to get a global map.

$$Y = \beta_0 + \beta_1 X_1 + \beta_2 X_2 + \dots + \beta_n X_n + \epsilon \quad (2)$$

where Y is the predicted ubRMSD, n the number of X_n geophysical condition (normalized descriptors) considered, β_n the corresponding coefficient, and ϵ the residuals.

The Variance Inflation Factor (VIF) (Belsley et al., 1980) method is used to quantify and filter the collinearities between all the descriptors in the regression. The threshold of more than 2.5 is set to assess whether the collinearity is too large in the regression (Johnston et al., 2017). The VIFs values are computed here as the diagonal elements of the inverse correlation matrix R_0 of the descriptors:

$$VIF = \text{diag}(R_0^{-1}) \quad (3)$$

4. Results

4.1. Assessment of SMOS using ISMN as reference

The SMOS L2SM ubRMSD obtained using the 1991 ISMN sensor time series are displayed in the histogram in Fig. 3 and in the map a) in Fig. 4. The histogram shows the ubRMSD distribution with a mean of $0.074 \text{ m}^3 \text{ m}^{-3}$, a median of $0.070 \text{ m}^3 \text{ m}^{-3}$, and the 25th and 75th quantiles of 0.057 and $0.087 \text{ m}^3 \text{ m}^{-3}$, respectively.

4.2. SMOS ubRMSD sensitivity to its footprint content

Fig. 3 shows a large range of ubRMSD values, which results from various factors such as the scale mismatch between the satellite footprint and the probe, the uncertainty of the probes (uncertainties, sampling depths) and the uncertainty of SMOS that we try to evaluate. We focus here on the effect of the surface conditions on the SMOS uncertainty. To evaluate this influence, Fig. 5 displays the distribution of ubRMSD as a function of different surface conditions within the SMOS footprint. Even though the relationships seem to follow some linear trend in most cases (correlation coefficients range between about 0.1 and 0.45), there is a notable dispersion around the fits. Regressions with the vegetation, topography, soil bulk density and soil organic carbon content exhibit the strongest correlations, whereas weaker relationships are observed for sand, clay, and open water bodies. In general, Fig. 5 shows that the

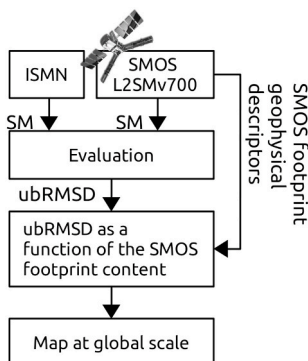


Fig. 1. Study overview.

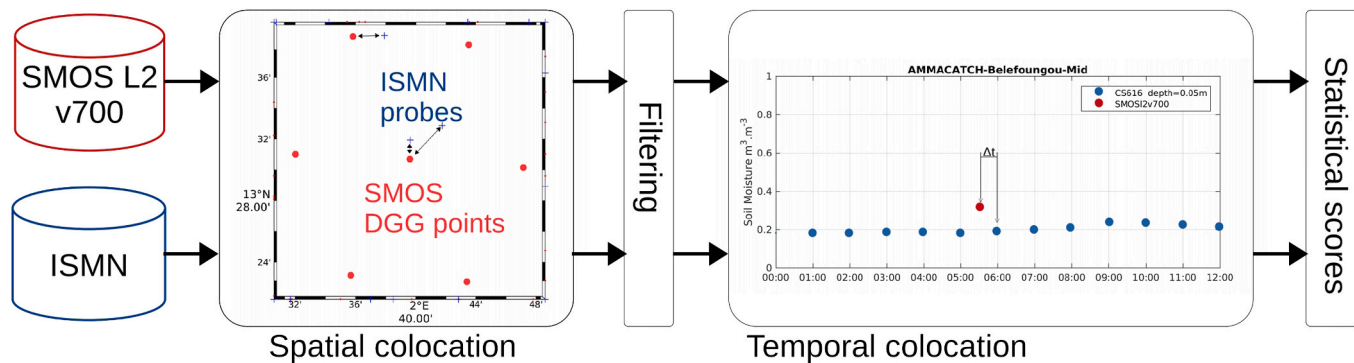


Fig. 2. Flowchart to assess the SMOS data using ISMN ground measurement as reference (SMOS DGG points is a SMOS grid node i.e. centre of the satellite footprint).

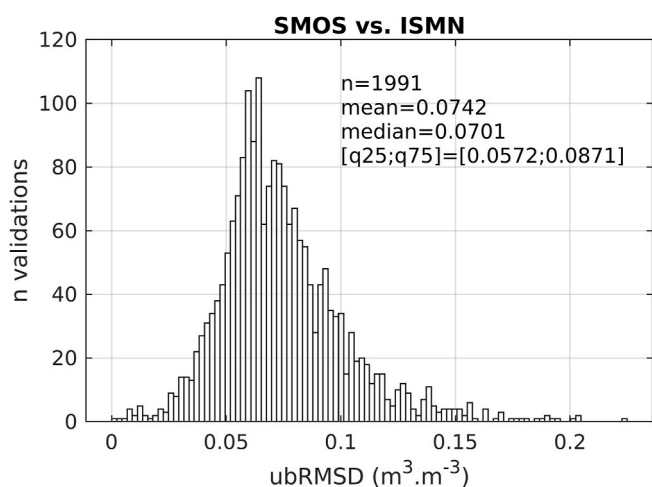


Fig. 3. Histogram of ubRMSD between SMOS and ISMN measurements.

higher the content of vegetation, clay, SOC, topography and open water bodies within the footprint, the worse the ubRMSD. In contrast, increasing sand content and bulk density leads to a better agreement with the *in situ* time series (lower ubRMSD).

4.3. A global uncertainty estimation as a function of surface conditions

4.3.1. Collinearity analysis

In Section 4.2, the SMOS uncertainty analysis is based on *in situ* sites, which do not equally represent all the global conditions due to their uneven spatial distribution. To extrapolate those relationships to a global scale, the method suggested here is to define a model based on a multiple linear regression, as described in the method section, that predicts the SMOS ubRMSD from the surface conditions within its footprint.

As descriptors can be interconnected in some way, their collinearities have to be analyzed before performing the regression. To assess those collinearities, the correlation matrix R_0 is presented in Fig. 6 where the Pearson correlation coefficients between permutations of the geophysical descriptors are shown (cases where p-value ≤ 0.05 are marked in bold font).

The correlation matrix shows that the vegetation descriptors defined as forest and low vegetation are highly and negatively correlated ($R = -0.98$), which is expected. A second couple of descriptors describing the topography (strong and moderate) are moderately linked ($R = 0.52$). A third relation can be identified by a moderate and negative relation between sand and clay values ($R = -0.55$).

The VIF coefficient is used to exclude strong collinearities from the regression (dark cells in Fig. 6). VIF values are ≤ 2.5 for the descriptor

clay (1.6), sand (1.5), bulk Density (1.5), SOC (1.9), open water (1.4), strong topography (1.4), and medium topography (1.5). However, the threshold of 2.5 is largely exceeded for the forest (46.1) and low vegetation (47.6). Consequently, we only kept forests as descriptors of the vegetation in the following analysis.

4.3.2. Map of SMOS uncertainty prediction at global scale

Section 4.3.1 presented the selection of the eight descriptors that are kept for the regression. The coefficients processed from the multiple linear regression described in the Method part are presented in Table 1.

The regression is then applied using the geophysical data presented in the Data section, at the global scale, to obtain the map b) displayed in Fig. 4. The red areas, where the ubRMSD is predicted as high ($> 0.1 \text{ m}^3 \text{ m}^{-3}$), correspond to areas where soil moisture retrieval is expected to be difficult. Clear patterns of relief, soil texture, and vegetation can be identified in Central Africa, Amazon, North America or Siberia. On the opposite, areas appear with better performances ($< 0.06 \text{ m}^3 \text{ m}^{-3}$), blue areas on the map, as in Australia, North and South Africa, Middle East or South America.

The histogram in Fig. 7 shows the SMOS ubRMSD distribution of all the pixels of the global map b) in Fig. 4. The distribution is characterized by a mean value of $0.076 \text{ m}^3 \text{ m}^{-3}$, a median at $0.072 \text{ m}^3 \text{ m}^{-3}$, a minimum/maximum at $0.018/0.19 \text{ m}^3 \text{ m}^{-3}$, an IQR_{25-75} of $0.031 \text{ m}^3 \text{ m}^{-3}$ and two modes, a first mode at $0.061 \text{ m}^3 \text{ m}^{-3}$ and a second one at $0.092 \text{ m}^3 \text{ m}^{-3}$.

5. Discussion

5.1. SMOS ubRMSD at ISMN sites

The analysis of SMOS ubRMSD at the *in situ* sites shows a wide range of score values (see Fig. 3). In addition to the SMOS uncertainties, these ubRMSD values include other sources of uncertainties, such as the ones characterizing the ground sensors and the scale mismatch between the sensors. Reviews on the intercomparison of different *in situ* probes (Ferrarezi et al., 2020; Rasheed et al., 2022) show a range of uncertainty from 0.01 to $0.04 \text{ m}^3 \text{ m}^{-3}$ and may vary with the probe technology, the calibration, and the set-up (soil type, air gap ...). The uncertainty resulting from the spatial scale between satellite and *in situ* measurements is an important factor in determining more precisely the actual uncertainty of SMOS SM. Microwave observations are characterized by their low spatial resolution of several hundreds of square kilometers, while the *in situ* measurements are representative of tens of centimeters around the probe. So, comparing the satellite data with the reference in heterogeneous areas can contribute strongly to the value of the metrics spread (Al Bitar et al., 2012; Colliander et al., 2021). In (Dorigo et al., 2021), authors estimate a probe's representativeness error between 0.03 and $0.05 \text{ m}^3 \text{ m}^{-3}$ by using the triple collocation method. The effect of heterogeneity of surface conditions in the satellite footprint on uncertainty assessment is complex in many respects. Heterogeneity increases

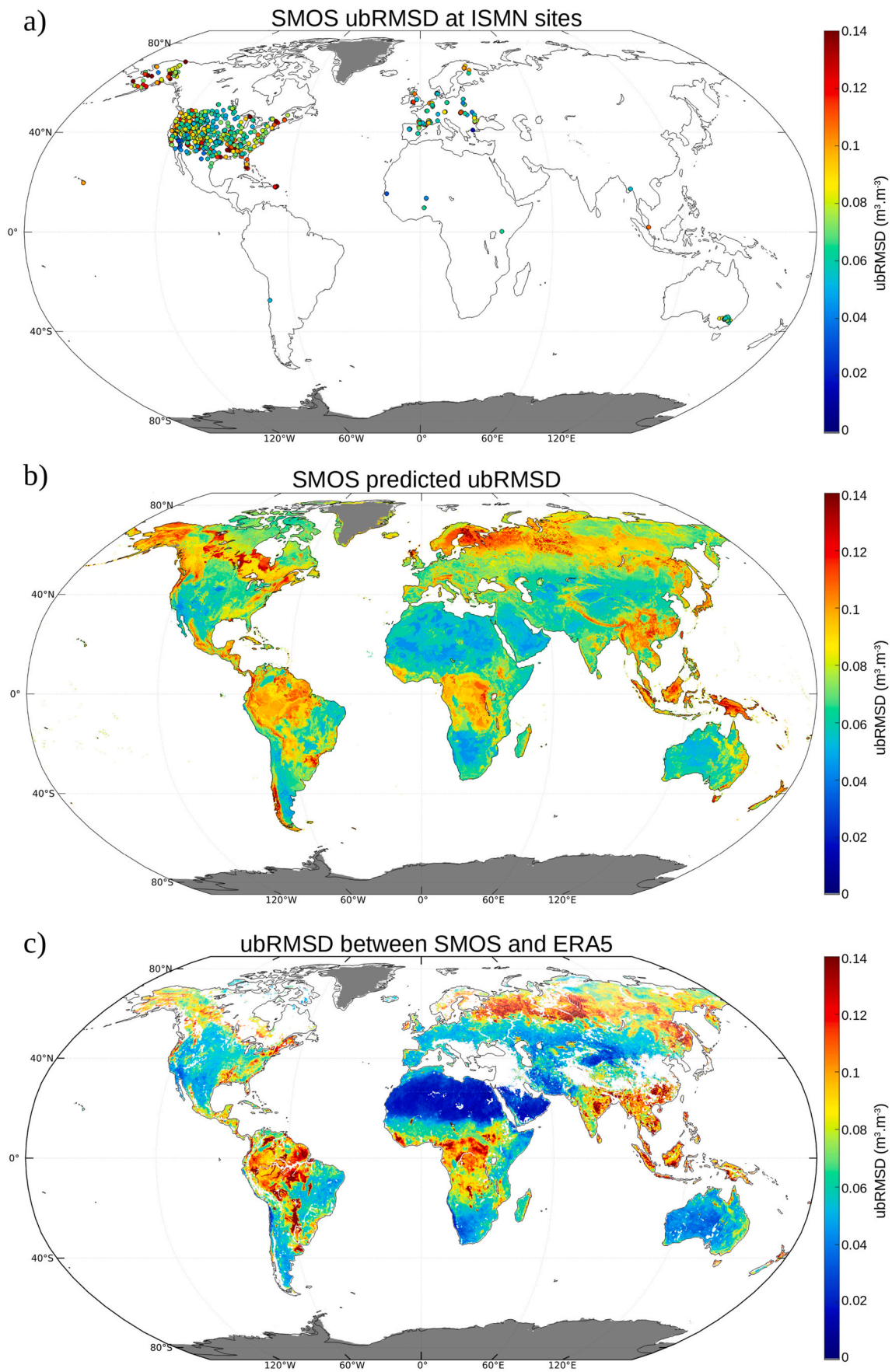


Fig. 4. a) Map of SMOS ubRMSD at each used ISMN site, b) Map of predicted SMOS ubRMSD related to surface condition ($\text{ubRMSD} = f(\text{vegetation, sand, clay, bulk density, SOC, open water bodies})$) and c) Map of ubRMSD of SMOS compared to ERA5 (QA4SM result, <https://doi.org/10.5281/zenodo.10018994>).

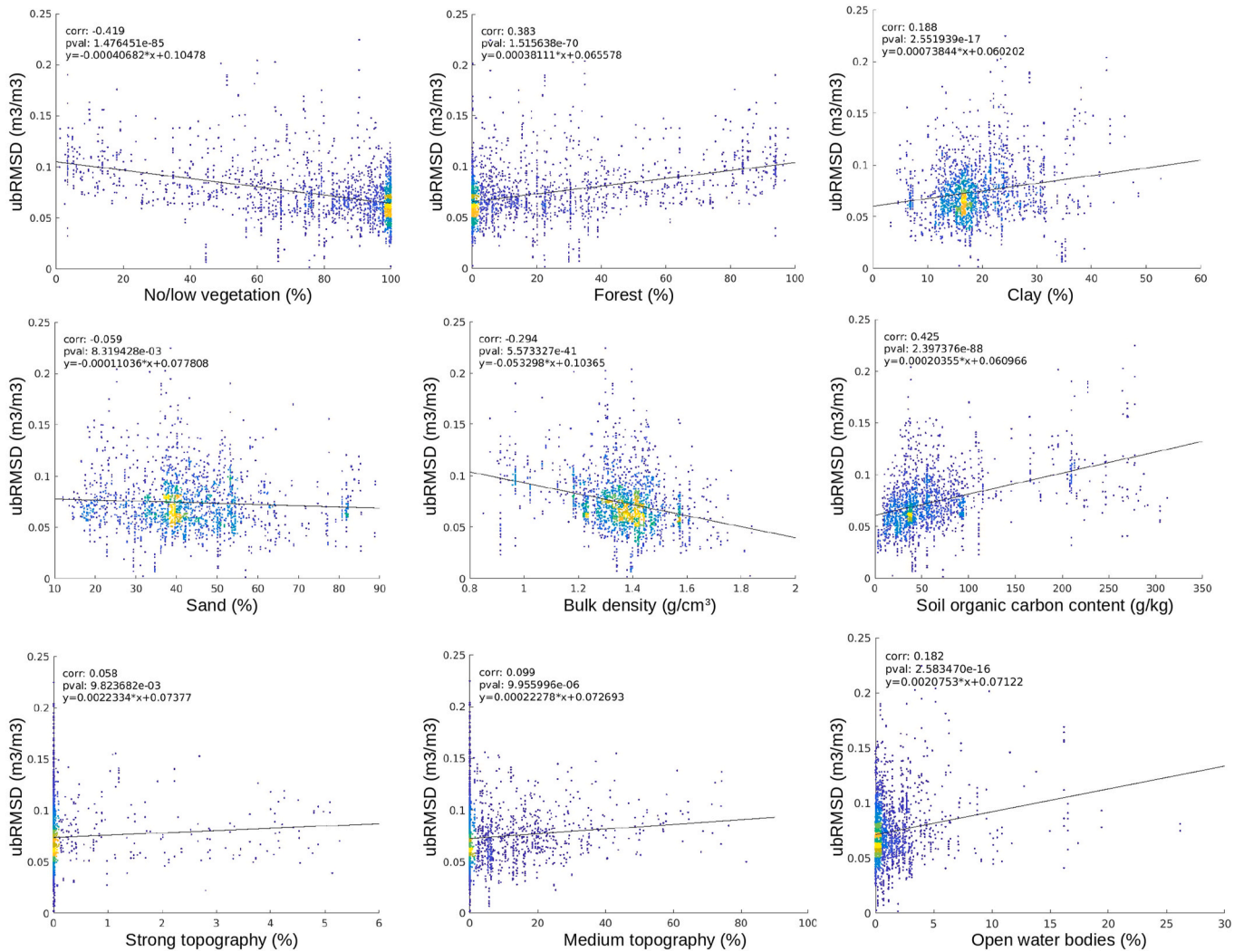


Fig. 5. Scatter plot showing the ubRMSD sensitivity to SMOS footprint content (the color corresponds to the density of validation points). (For interpretation of the references to color in this figure legend, the reader is referred to the Web version of this article.)

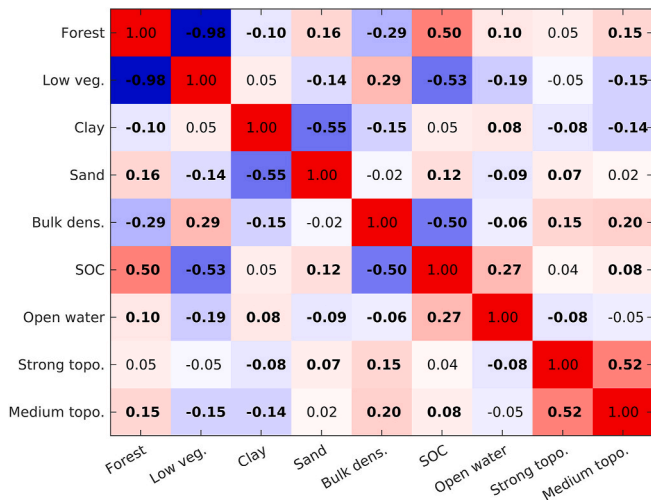


Fig. 6. Collinearities between the geophysical descriptors used to characterize the SMOS footprint, the color strength is linked to the correlation strength displayed in all cases (the darker, the higher). (For interpretation of the references to color in this figure legend, the reader is referred to the Web version of this article.)

Table 1

Coefficients, and their SE in bracket, used to relate the SMOS ubRMSD and the surface condition. SE stand for the standard error.

Descriptor X	Coef.	Value (SE)
Intercept	β_0	7.42e-2 (5.24e-4)
Vegetation	β_1	6.7e-3 (6.20e-4)
Clay	β_2	4.94e-3 (6.49e-4)
Sand	β_3	-6.18e-4 (6.46e-4)
Soil density	β_4	-2.86e-3 (6.45e-4)
SOC	β_5	5.89e-3 (7.15e-4)
Open water	β_6	2.23e-3 (5.57e-4)
Strong topo.	β_7	1.02e-3 (6.19e-4)
Moderate topo.	β_8	2.09e-3 (6.45e-4)

the complexity of surface emissions modeling, which can increase the uncertainty of the derived soil moisture. In addition, increasing surface heterogeneity increases the spatial scale mismatch between the spatial scale monitored by the probe and the satellite field of view. However, it is challenging to define the heterogeneity as it is made up of different aspects, such as the level of diversity of surface conditions or the spatial distribution of these conditions. While many methods exist to assess the level of diversity (such as the Gini-Simpson index used in (Wang et al., 2024) or (Kim et al., 2023)), taking into account the spatial distribution is still not sufficiently understood. Consequently, the ubRMSD

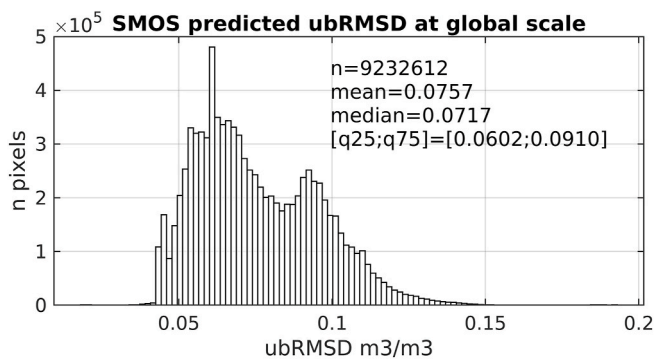


Fig. 7. Histogram of the predicted SMOS ubRMSD map b) Fig. 4.

(histogram in Fig. 3) should be interpreted as the upper bound estimate of the SMOS uncertainty, which includes the other sources not linked to the SMOS performances.

5.2. Uncertainty at the global scale

5.2.1. Caveats and limits of the method

The statistical relationships derived between the ubRMSD and the different surface conditions are not very uniform, see Fig. 5. Indeed, (Dorigo et al., 2021) showed that the ISMN network locations are uneven and do not cover all climate conditions. It implies that the relationships in Fig. 5 may not be well-defined for all the range of the predictors. For instance, no SM measurements are available in tropical forest (top panel, middle column Fig. 5), i.e. more ubRMSD are computed with forest fraction lower than 40% than above. *In situ* data in these environments would equalize the ubRMSD for all fraction conditions, and thus enhance the quality of the regression.

One should also be aware of the risks of the presence of RFI (especially in the Middle East and Asia in general). They are not directly represented on the map b) in Fig. 4 but indirectly within the filtering of the SMOS data. The probability of RFI that is available in the SMOS data, can not be related to neither the intensity of these RFI, nor their impacts in terms of SM.

For the purpose of this study, we used static data, as a first attempt. The temporal variability of variables such as the vegetation, or snow, will be included in further study.

5.2.2. Sensitivity of satellite observations to footprint content

The presence of vegetation within the footprint increases the ubRMSD, as shown by the trends on the two top panels in Fig. 5. This vegetation effect is well known and documented (Jackson and Schmugge, 1991; Mätzler, 1994; Hornbuckle et al., 2003; van der Schalie et al., 2017), it is less important at L-band than C or X-band (Frappart et al., 2020). In the microwave radiometry domain, the vegetation water content attenuates the signal coming from the underlying surface and contributes to TB through its temperature and emissivity. So a vegetation layer decreases the sensitivity of passive microwave TB to the underneath surface. As a consequence, the denser the vegetation is, the less sensitive the satellite measurements (TB) are to soil moisture, which increases its uncertainty.

The presence of complex topography within the footprint is also deteriorating the scores, as shown on the panel "Moderate topography" and "Strong topography" in Fig. 5. It affects strongly the passive microwave measurements as local incidence angles are different from a flat surface, and mixes the polarizations, hampering any accurate SM retrieval. As the effect of topography can not be easily quantified, we rely on the fraction of the footprint that is subject to complex topography (Pellarin et al., 2016; Kerr et al., 2003; Mialon et al., 2008). In consequence, high ubRMSD is then expected for areas with strong topography.

This study sheds light on the influence of the soil texture on the ubRMSD scores considering the soil bulk density. The ubRMSD significantly depends on the bulk density at SMOS scale, with results showing lower ubRMSD with increasing bulk density (Fig. 5). Indeed, high bulk density reduces the dynamic of the soil moisture, leading to a decrease in the ubRMSD (Pan et al., 2022). One explanation is with increasing bulk density, the volume of soil particle increases, reducing the available volume for air and water. Moreover, the contact of the probes pin and the soil may alter in soil with low bulk density (Matula et al., 2016), which could impact the quality of the ground measurements.

In Fig. 5 the relation between the soil organic carbon content within the SMOS footprint and the ubRMSD shows a worsening of the ubRMSD when the SOC content is increasing. This trend can be attributed to three factors. First, the SOC has an impact on the dielectric constant and a particular model was developed, and implemented in the SMOS retrieval (Bircher et al., 2016a). Second, a dedicated calibration of the probes is needed in high SOC context (Bircher et al., 2016b), which is not always done. Finally, and in agreement with the trend found in this study (see Fig. 6), the potential of soil organic activity is positively related to a reduction of the bulk-density (Aşkin and Özdemir, 2003).

Sand and clay have opposite effects, as the relationships show an improvement (decrease of ubRMSD) with sandy soil and a worsening (increase of ubRMSD) with clayey soil, as shown in Fig. 5. The worsening of the score in clay soil can be attributed to three factors. First, the dielectric constant model used in the SMOS, even though (Mironov et al., 2013) showed an adaption of the model to various clay conditions. Second, the *in situ* probe calibration law in the very clayey area is still an issue (SU et al., 2014; Gong et al., 2003), since some specific soil textures (like high clay soils) are often not considered in standard calibration functions. Finally, there is a risk of poor pin-soil contact due to the crackling of the soil matrix during dry periods (Reid and Parkinson, 1984).

The presence of open water bodies is also strongly worsening the scores. In fact, open water bodies impacts the radiometric signal due to the very low emissivity of water when compared to soils and vegetation (Ulaby et al., 1981). In the map b) in Fig. 4, the high ubRMSD expected in the northern part of North America (the darkest areas) is attributed to these water fractions. Water bodies are highly present in the SMOS field of view in these regions, which makes the SM retrieval complex. It implies that the water maps used to delimit these water bodies have to be very accurate in these areas, which may not always be the case, as the extent of these open waters bodies is dynamic throughout the year whereas SMOS land cover maps are static.

5.2.3. Evaluation of the global ubRMSD

The challenge is to evaluate the consistency of the predicted ubRMSD (map b) in Fig. 4). The global map displays spatial patterns that are expected, such as higher ubRMSD ($\sim 0.1 \text{ m}^3 \text{ m}^{-3}$) in dense forest areas. The global pattern can also be compared with studies estimating SMOS error based on a triple collocation method, such as Australia in (Bhardwaj et al., 2022) or at a global scale in (Leroux et al., 2013). Both studies support the spatial distribution that is obtained in map b) in Fig. 4. Other studies in the literature offer analysis in various conditions. For example, the authors in (Xu and Frey, 2021) found an ubRMSD within the range $0.04\text{--}0.07 \text{ m}^3 \text{ m}^{-3}$ against *in situ* probes around the Laurentian Great Lakes basin, where we estimate the ubRMSD in the range $0.05\text{--}0.09 \text{ m}^3 \text{ m}^{-3}$. In (Jamei et al., 2020) an evaluation in Iran found an ubRMSD of $0.039\text{--}0.06 \text{ m}^3 \text{ m}^{-3}$ comparable to our predicted ubRMSD ($0.04\text{--}0.1 \text{ m}^3 \text{ m}^{-3}$). In (Kang et al., 2019), SMOS ubRMSD was estimated between 0.05 and $0.12 \text{ m}^3 \text{ m}^{-3}$ in Malaysia, where ours range from 0.06 to $0.11 \text{ m}^3 \text{ m}^{-3}$. Differences with findings from the literature are expected as the validation strategies (the selection of the *in situ* sites) may change, but our results agree well with the existing studies.

Two other approaches are proposed to assess the uncertainties of the map b) in Fig. 4. First, we use the estimations obtained at the ISMN sites, which are compared to the uncertainties obtained from the direct

comparison of SMOS SM and the ISMN *in situ* measurements (see Section 4.1). The histogram in Fig. 7 shows a distribution that is quite similar to the histogram in Fig. 3. A second mode at $0.088 \text{ m}^3\text{m}^{-3}$ is observed in Fig. 7, which is related to the vegetation areas and their impact on the ubRMSD. Indeed, dense vegetation was not considered in the analysis that led to the histogram in Fig. 3 due to the lack of *in situ* measurement under forest conditions. Another comparison is made in Fig. 8, comparing the ubRMSD at the ISMN sites and the predicted ones also at the *in situ* sites. The predicted ubRMSD (y-axis) are well in line with the uncertainty of SMOS at the *in situ* sites (x-axis) as the distribution of the points is around the 1:1 line.

Second, the validation platform Quality Assurance for Soil Moisture (QA4SM) was used to derive a global comparison between SMOS L2v700 and ERA5. The result is shown in map c) in Fig. 4. The empty areas on the map c) in Fig. 4 are probably linked to RFI sources, well known in these areas. Even though it is not a direct validation, it is useful to support our findings as one can notice the good spatial agreement between the two maps, which also exhibit similar orders of magnitude. This comparison has to be taken with care, as it does not reflect the “absolute” SMOS performances, and ERA5 bears its uncertainties.

5.2.4. Analysis of global ubRMSD

Even though the ubRMSD is an upper limit of SMOS ubRMSD, it presents spatial patterns that are coherent and provides an absolute ubRMSD where it was not available before. Areas with low or dry vegetation have an ubRMSD lower than $0.05 \text{ m}^3\text{m}^{-3}$. Higher ubRMSD are found in denser vegetated areas (tropical and boreal forests) where the derived ubRMSD can reach $0.12 \text{ m}^3\text{m}^{-3}$.

Satellite missions that estimate soil moisture such as SMOS or SMAP, have specifications in terms of expected accuracy, that is less than or equal to $0.04 \text{ m}^3\text{m}^{-3}$ over homogeneous areas with vegetation water content less than 5 kg/m^2 . This specification is based on previous experiments on the ability of soil moisture retrieval from L-band microwave radiometer (Kerr, 1998) and on the needs of the hydrological application (Chanzy et al., 1995). The map b) in Fig. 4 shows the areas where our method suggests the $0.04 \text{ m}^3\text{m}^{-3}$ are met, i.e. North Africa, Western Australia, South Africa. These areas may seem limited, but one should take into account that this uncertainty is the upper limit, as it does not represent only the satellite uncertainty but the contribution of all the sources (satellite, ground measurement, and scale mismatch).

Our results can be useful to better assess the mission requirements and the related surface conditions of future missions. SMOS and SMAP are still providing important knowledge of the water cycle, but are several years into their mission, and the community is defining the follow-up of these missions to ensure the continuity of SM observations by satellite (Rodríguez-Fernández et al., 2024).

6. Conclusion

In this study, we performed an analysis of passive microwave soil moisture uncertainty as a function of surface conditions. SMOS is used to support our approach, and its performance is assessed in a first part, using the ISMN network as a reference (Section 4.1). Results show a large variability of ubRMSD values (with a median of $0.070 \text{ m}^3\text{m}^{-3}$ and an interquartile range of $0.030 \text{ m}^3\text{m}^{-3}$). The investigation in Section 4.2 shows a dependence of the SMOS uncertainty on the land surface characteristics within the satellite footprint. The results show a clear improvement of the scores when the footprint scene is mainly flat and does not contain either open water bodies (e.g., lakes) or forests. Soil parameters also impact the scores, which are best for sandier, high bulk-density soils and low soil organic carbon content. This study then suggests that we can approximate SMOS uncertainty at the global scale by considering the relationship between the geophysical SMOS footprint content and the validation scores (Section 4.3). The predicted SMOS ubRMSD values are consistent with the literature, and an evaluation with ERA5 supports the proposed approach. This map is a first attempt

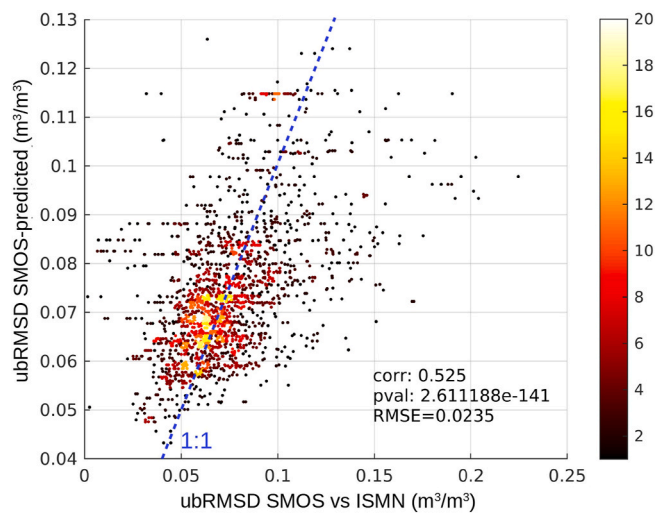


Fig. 8. Comparison of the ubRMSD obtained by the analysis SMOS vs. ISMN (x-axis) and the predicted ones at global scale (y-axis).

to estimate SMOS soil moisture retrieval performances at the global scale using the surface condition, and to provide an estimation of SMOS uncertainty over areas where no ground reference exists.

This study will be further developed with a focus on the spatial distribution such as the scale mismatch between low resolution satellite and very local measurements, the heterogeneity of the geophysical parameters within the footprint on the SMOS soil moisture performances, and the temporal influence (i.e. using weekly/monthly soil moisture averages for instance). SMOS was chosen to support our approach, but it can be applied to other satellite sensors, including the ones of interest for our case, i.e. SMAP and SMOS.

CRedit authorship contribution statement

François Gibon: Writing – review & editing, Writing – original draft, Software, Methodology, Investigation, Conceptualization. **Arnaud Mialon:** Writing – review & editing, Writing – original draft, Methodology, Investigation, Conceptualization. **Philippe Richaume:** Writing – review & editing, Methodology, Investigation, Conceptualization. **Nemesio Rodríguez-Fernández:** Writing – review & editing. **Daniel Aberer:** Resources. **Alexander Boresch:** Supervision. **Raffaele Crapolicchio:** Project administration, Funding acquisition. **Wouter Dorigo:** Writing – review & editing. **Alexander Gruber:** Writing – review & editing. **Irene Himmelbauer:** Writing – review & editing. **Wolfgang Preimesberger:** Writing – review & editing. **Roberto Sabia:** Project administration, Funding acquisition. **Pietro Stradiotti:** Resources. **Monika Tercjak:** Resources. **Yann H. Kerr:** Writing – review & editing.

Declaration of competing interest

The authors declare that they have no known competing financial interests or personal relationships that could have appeared to influence the work reported in this paper.

Data availability

Data will be made available on request.

Acknowledgements

This work was supported by the European Space Agency (ESA) in the context of the Fiducial Reference Measurement for Soil Moisture (FRM4SM) project (project contract n°4000135204/21//I-BG), the Centre National d'Études Spatiale (CNES), the Terre solide, Océan,

Appendix A. List of the ISMN networks used in this study

AMMA-CATCH (Lebel et al., 2009)	ARM (Phillips et al., 2017)
BIEBRZA-S-1 (Dabrowska-Zielinska et al., 2018)	BNZ-LTER (Van Cleve et al., 2015)
CTP-SMTMN (Yang et al., 2013)	COSMOS (Zreda et al., 2012)
DAHRA (Tagesson et al., 2014)	FLUXNET-AMERIFLUX
FMI (Ikonen et al., 2018)	FR-Aqui (Al-Yaari et al., 2018)
GROW (Xaver et al., 2020)	GTK
HOBE (Jensen and Refsgaard, 2018)	HYDROL-NET-PERUGIA (Morbideilli et al., 2011)
ICN (Hollinger and Isard, 1994)	IIT-KANPUR
IMA-CANI (Capello et al., 2019)	IPE (Alday et al., 2020)
IRON (Osenga et al., 2021)	LAB-net (Mattar et al., 2016)
METEROBS	MOL-RAO (Beyrich and Adam, 2007)
MySMNet (Kang et al., 2019)	ORACLE
OZNET (Smith et al., 2012)	PBO-H2O (Larson et al., 2008)
REMEDHUS (González-Zamora et al., 2019)	RISMA (Ojo et al., 2015)
RSMN	SCAN (Schaefer et al., 2007)
SMOSMANIA (Calvet et al., 2016)	SNOTEL (Leavesley, 2010)
SOILSCAPE (Moghaddam et al., 2016)	SWEX-POLAND (Marczewski et al., 2010)
TERENO (Bogena, 2016)	UDC-SMOS (Schlenz et al., 2012)
USCRN (Bell et al., 2013)	VAS
VDS	WSMN (Petropoulos and McCalmont, 2017)

References

- Al Bitar, A., Leroux, D., Kerr, Y.H., Merlin, O., Richaume, P., Sahoo, A., Wood, E.F., 2012. Evaluation of smos soil moisture products over continental u.s. using the scan/snotel network. *IEEE Trans. Geosci. Rem. Sens.* 50 (5), 1572–1586. <https://doi.org/10.1109/TGRS.2012.2186581>.
- Al-Yaari, A., Dayau, S., Chipeaux, C., Aluome, C., Kruszewski, A., Loustau, D., Wigneron, J.-P., 2018. The aqui soil moisture network for satellite microwave remote sensing validation in south-western France. *Rem. Sens.* 10 (11) <https://doi.org/10.3390/rs10111839>.
- Al-Yaari, A., Wigneron, J.-P., Dorigo, W., Colliander, A., Pellarin, T., Hahn, S., Mialon, A., Richaume, P., Fernandez-Moran, R., Fan, L., Kerr, Y., De Lannoy, G., 2019. Assessment and inter-comparison of recently developed/reprocessed microwave satellite soil moisture products using ismn ground-based measurements. *Rem. Sens. Environ.* 224, 289–303. <https://doi.org/10.1016/j.rse.2019.02.008>.
- Albergel, C., de Rosnay, P., Gruhier, C., Muñoz-Sabater, J., Hasenauer, S., Isaksen, L., Kerr, Y.H., Wagner, W., 2012. Evaluation of remotely sensed and modelled soil moisture products using global ground-based in situ observations. *Rem. Sens. Environ.* 118, 215–226. <https://doi.org/10.1016/j.rse.2011.11.017>.
- Alday, J.G., Camarero, J.J., Revilla, J., Resco de Dios, V., 2020. Similar diurnal, seasonal and annual rhythms in radial root expansion across two coexisting Mediterranean oak species. *Tree Physiol.* 40 (7), 956–968. <https://doi.org/10.1093/treephys/tpaa041>.
- Aşkin, T., Özdemir, N., 2003. Soil bulk density as related to soil particle size distribution and organic matter content. *Poljoprivreda/Agriculture* 9, 52–55.
- Bell, J., Palecki, M., Baker, B., Collins, W., Lawrimore, J., Leeper, R., Hall, M., Kochendorfer, J., Meyers, T., Wilson, T., Diamond, H., 2013. U.S. climate reference network soil moisture and temperature observations. *J. Hydrometeorol.* 14, 977–988. <https://doi.org/10.1175/JHM-D-12-0146.1>.
- Belsley, D.A., Kuh, E., Welsch, R.E., 1980. *Regression Diagnostics*. Wiley. <https://doi.org/10.1002/0471725153>.
- Beyrich, F., Adam, W., 2007. Site and data report for the lindenber reference site in ceop - phase 1, *berichte des deutschen wetterdienstes*, 230, p. 2007 offenbach am main.
- Bhardwaj, J., Kuleshov, Y., Chua, Z.-W., Watkins, A.B., Choy, S., Sun, Q.C., 2022. Evaluating satellite soil moisture datasets for drought monitoring in Australia and the south-west pacific. *Rem. Sens.* 14 (16), 3971. <https://doi.org/10.3390/rs14163971>.
- Bircher, S., Demontoux, F., Razafindratsima, S., Zakharova, E., Drusch, M., Wigneron, J.-P., Kerr, Y.H., 2016a. L-band relative permittivity of organic soil surface layers—a new dataset of resonant cavity measurements and model evaluation. *Rem. Sens.* 8 (12), 1024. <https://doi.org/10.3390/rs8121024>.
- Bircher, S., Andreasen, M., Vuollet, J., Vehviläinen, J., Rautiainen, K., Jonard, F., Weihermüller, L., Zakharova, E., Wigneron, J.-P., Kerr, Y.H., 2016b. Soil moisture sensor calibration for organic soil surface layers. *Geoscientific instrumentation, methods and data systems* 5 (1), 109–125. <https://doi.org/10.5194/gi-5-109-2016>.
- Bogena, H.R., 2016. Tereno: German network of terrestrial environmental observatories. *Journal of large-scale research facilities JLSRF* 2, A52. <https://doi.org/10.17815/jlsrf-2-98>.
- Bolten, J.D., Crow, W.T., Zhan, X., Jackson, T.J., Reynolds, C.A., 2010. Evaluating the utility of remotely sensed soil moisture retrievals for operational agricultural drought monitoring. *IEEE J. Sel. Top. Appl. Earth Obs. Rem. Sens.* 3 (1), 57–66. <https://doi.org/10.1109/JSTARS.2009.2037163>.
- Calvet, J.-C., Fritz, N., Berne, C., Piguet, B., Maurel, W., Meurey, C., 2016. Deriving pedotransfer functions for soil quartz fraction in southern France from reverse modeling. *SOIL* 2 (4), 615–629. <https://doi.org/10.5194/soil-2-615-2016>.
- Capello, G., Biddoccu, M., Ferraris, S., Cavallo, E., 2019. Effects of tractor passes on hydrological and soil erosion processes in tilled and grassed vineyards. *Water* 11 (10), 2118. <https://doi.org/10.3390/w11102118>.
- Chanzy, A., Bruckler, L., Perrier, A., 1995. Soil evaporation monitoring: a possible synergism of microwave and infrared remote sensing. *J. Hydrol.* 165 (1–4), 235–259.
- Colliander, A., Reichle, R., Crow, W., Cosh, M.H., Chen, F., Chan, S.K., Das, N.N., Bindlish, R., Chaubell, M.J., Kim, S., Liu, Q., Oneill, P.E., Dunbar, S., Dang, L.B., Kimball, J.S., Jackson, T.J., Aljassar, H.K., Asanuma, J., Bhattacharya, B.K., Berg, A., Bosch, D.D., Bourgeau-Chavez, L.L., Caldwell, T., Calvet, J.-C., Collins, C.H., Jensen, K.H., Livingston, S., Lopez-Baeza, E., Martinez-Fernandez, J., McNairn, H., Moghaddam, M., Montzka, C., Notarnicola, G., Pellarin, T., Pfeil, I., Pulliainen, J., Ramos, J., Seyfried, M., Starks, P., Su, B., der Velde, R.V., Zeng, Y., Thibeault, M., Vreugdenhil, M., Walker, J.P., Zribi, M., Entekhabi, D., Yueh, S.H., 2021. Validation of soil moisture data products from the NASA SMAP mission. *IEEE J. Sel. Top. Appl. Earth Obs. Rem. Sens.* 1. <https://doi.org/10.1109/jstars.2021.3124743>.
- Colliander, A., Kerr, Y., Wigneron, J., Al-Yaari, A., Rodriguez-Fernandez, N., Li, X., Chaubell, J., Richaume, P., Mialon, A., Asanuma, J., et al., 2023. Performance of smos soil moisture products over core validation sites. *Geosci. Rem. Sens. Lett. IEEE*. <https://doi.org/10.1109/LGRS.2023.3272878>.
- Dabrowska-Zielinska, K., Musial, J., Malinska, A., Budzyska, M., Gurdak, R., Kiryla, W., Bartold, M., Grzybowski, P., 2018. Soil moisture in the biebza wetlands retrieved from sentinel-1 imagery. *Rem. Sens.* 10 (12), 1979. <https://doi.org/10.3390/rs10121979>.
- Dorigo, W., Himmelbauer, I., Aberer, D., Schremmer, L., Petrakovic, I., Zappa, L., Preimesberger, W., Xaver, A., Annor, F., Ardó, J., Baldocchi, D., Bitelli, M., Blöschl, G., Bogena, H., Brocca, L., Calvet, J.-C., Camarero, J.J., Capello, G., Choi, M., Cosh, M.C., van de Giesen, N., Hajdu, I., Ikonen, J., Jensen, K.H., Kanniah, K.D., de Kat, I., Kirchengast, G., Kumar Rai, P., Kyrouac, J., Larson, K., Liu, S., Loew, A., Moghaddam, M., Martínez Fernández, J., Mattar Bader, C., Morbidelli, R., Musial, J.P., Osenga, E., Palecki, M.A., Pellarin, T., Petropoulos, G.P., Pfeil, I., Powers, J., Robock, A., Rüdiger, C., Rummel, U., Strobel, M., Su, Z., Sullivan, R., Tagesson, T., Varlagin, A., Vreugdenhil, M., Walker, J., Wen, J., Wenger, F., Wigneron, J.P., Woods, M., Yang, K., Zeng, Y., Zhang, X., Zreda, M., Dietrich, S., Gruber, A., van Oevelen, P., Wagner, W., Scipal, K., Drusch, M., Sabia, R., 2021. The international soil moisture network: serving earth system science for over a decade. *Hydrol. Earth Syst. Sci.* 25 (11), 5749–5804. <https://doi.org/10.5194/hess-25-5749-2021>.
- Douville, H., Chauvin, F., 2000. Relevance of soil moisture for seasonal climate predictions: a preliminary study. *Clim. Dynam.* 16 (10), 719–736. <https://doi.org/10.1007/s003820000080>.
- Drusch, M., 2007. Initializing numerical weather prediction models with satellite-derived surface soil moisture: data assimilation experiments with ecmwf's integrated forecast system and the tmi soil moisture data set. *J. Geophys. Res. Atmos.* 112 (D3) <https://doi.org/10.1029/2006JD007478>.
- Entekhabi, D., Njoku, E.G., O'Neill, P.E., Kellogg, K.H., Crow, W.T., Edelstein, W.N., Entin, J.K., Goodman, S.D., Jackson, T.J., Johnson, J., Kimball, J., Piepmeier, J.R., Koster, R.D., Martin, N., McDonald, K.C., Moghaddam, M., Moran, S., Reichle, R., Shi, J.C., Spencer, M.W., Thurman, S.W., Tsang, L., Van Zyl, J., 2010. The soil

- moisture active passive (smap) mission. Proc. IEEE 98 (5), 704–716. <https://doi.org/10.1109/JPROC.2010.2043918>.
- F. G., 2008. Global Agro-Ecological Zones Assessment for Agriculture (Gaez 2008). iiasa, laxenburg, austria and fao, rome, italy.
- Ferrarezi, R.S., Nogueira, T.A.R., Zepeda, S.G.C., 2020. Performance of soil moisture sensors in Florida sandy soils. Water 12 (2), 358. <https://doi.org/10.3390/w12020358>.
- Frappart, F., Wigneron, J.-P., Li, X., Liu, X., Al-Yaari, A., Fan, L., Wang, M., Moisy, C., Le Masson, E., Aoulad Lafkih, Z., Vallé, C., Ygorra, B., Baghdadi, N., 2020. Global monitoring of the vegetation dynamics from the vegetation optical depth (vod): a review. Rem. Sens. 12 (18) <https://doi.org/10.3390/rs12182915>.
- Gibon, F., Pellarin, T., Román-Cascón, C., Alhassane, A., Traoré, S., Kerr, Y.H., Seen, D.L., Baron, C., 2018. Millet yield estimates in the sahel using satellite derived soil moisture time series. Agric. For. Meteorol. 262, 100–109. <https://doi.org/10.1016/j.agrformet.2018.07.001>.
- Gong, Y., Cao, Q., Sun, Z., 2003. The effects of soil bulk density, clay content and temperature on soil water content measurement using time-domain reflectometry. Hydrol. Process. 17 (18), 3601–3614. <https://doi.org/10.1002/hyp.1358>.
- González-Zamora, A., Sánchez, N., Pablos, M., Martínez-Fernández, J., 2019. Cci soil moisture assessment with smos soil moisture and in situ data under different environmental conditions and spatial scales in Spain. Rem. Sens. Environ. 225, 469–482. <https://doi.org/10.1016/j.rse.2018.02.010>.
- Gruber, A., De Lannoy, G., Albergel, C., Al-Yaari, A., Brocca, L., Calvet, J.-C., Colliander, A., Cosh, M., Crow, W., Dorigo, W., et al., 2020a. Validation practices for satellite soil moisture retrievals: what are (the) errors? Rem. Sens. Environ. 244, 111806 <https://doi.org/10.1016/j.rse.2020.111806>.
- Gruber, A., Lannoy, G.D., Albergel, C., Al-Yaari, A., Brocca, L., Calvet, J.-C., Colliander, A., Cosh, M., Crow, W., Dorigo, W., Draper, C., Hirschi, M., Kerr, Y., Konings, A., Lahoz, W., McColl, K., Montzka, C., Muñoz-Sabater, J., Peng, J., Reichle, R., Richaume, P., Rüdiger, C., Scanlon, T., van der Schalie, R., Wigneron, J.-P., Wagner, W., 2020b. Validation practices for satellite soil moisture retrievals: what are (the) errors? Rem. Sens. Environ. 244, 111806 <https://doi.org/10.1016/j.rse.2020.111806>.
- Hersbach, H., Bell, B., Berrisford, P., Biavati, G., Horányi, A., Muñoz Sabater, J., Nicolas, J., Peubey, C., Radu, R., Rozum, I., Schepers, D., Simmons, A., Soci, C., Dee, D., Thépaut, J.-N., 2018. Era5 hourly data on single levels from 1959 to present. copernicus climate change service (c3s) climate data store (cds). <https://doi.org/10.24381/cds.adbb2d47>.
- Hollinger, S., Isard, S., 1994. A soil moisture climatology of Illinois. J. Clim. 7, 822–833.
- Hornbuckle, B.K., England, A.W., De Roo, R.D., Fischman, M.A., Boprie, D.L., 2003. Vegetation canopy anisotropy at 1.4 ghz. IEEE Trans. Geosci. Rem. Sens. 41 (10), 2211–2223. <https://doi.org/10.1109/TGRS.2003.817192>.
- Ikonen, J., Smolander, T., Rautiainen, K., Cohen, J., Lemmetyinen, J., Salminen, M., Pulliainen, J., 2018. Spatially distributed evaluation of esa cci soil moisture products in a northern boreal forest environment. Geosciences 8 (2). <https://doi.org/10.3390/geosciences8020051>.
- Jackson, T., Schmugge, T., 1991. Vegetation effects on the microwave emission of soils. Rem. Sens. Environ. 36 (3), 203–212. [https://doi.org/10.1016/0034-4257\(91\)90057-D](https://doi.org/10.1016/0034-4257(91)90057-D).
- Jamei, M., Baygi, M.M., Oskouei, E.A., Lopez-Baeza, E., 2020. Validation of the SMOS level 1c brightness temperature and level 2 soil moisture data over the west and southwest of Iran. Rem. Sens. 12 (17), 2819. <https://doi.org/10.3390/rs12172819>.
- Jensen, K.H., Refsgaard, J.C., 2018. Hobe: the Danish hydrological observatory. Vadose Zone J. 17 (1), 180059 arXiv. <https://access.onlinelibrary.wiley.com/doi/pdf/10.2136/vzj2018.03.0059>, 10.2136/vzj2018.03.0059.
- Johnston, R., Jones, K., Manley, D., 2017. Confounding and collinearity in regression analysis: a cautionary tale and an alternative procedure, illustrated by studies of british voting behaviour. Qual. Quantity 52 (4), 1957–1976. <https://doi.org/10.1007/s11135-017-0584-6>.
- Kang, C.S., Kanniah, K.D., Kerr, Y.H., 2019. Calibration of smos soil moisture retrieval algorithm: a case of tropical site in Malaysia. IEEE Trans. Geosci. Rem. Sens. 57 (6), 3827–3839. <https://doi.org/10.1109/TGRS.2018.2888535>.
- Kerr, Y., 1998. The Smos Mission: Miras on Ramses. A Proposal to the Call for Earth Explorer Opportunity Mission.
- Kerr, Y.H., 2006. Soil moisture from space: where are we? Hydrogeol. J. 15 (1), 117–120. <https://doi.org/10.1007/s10040-006-0095-3>.
- Kerr, Y.H., Secherre, F., Lastenet, J., Wigneron, J.-P., 2003. Smos: analysis of perturbing effects over land surfaces. In: IGARSS 2003. 2003 IEEE International Geoscience and Remote Sensing Symposium. Proceedings (IEEE Cat. No.03CH37477), 2, pp. 908–910. <https://doi.org/10.1109/IGARSS.2003.1293960> vol. 2.
- Kerr, Y.H., Waldteufel, P., Wigneron, J.-P., Delwart, S., Cabot, F., Boutin, J., Escorihuela, M., Font, J., Reul, J., Gruhier, C., Enache Juglea, S., Drinkwater, M.R., Hahne, A., Martin Neira, M., Mecklenburg, S., 2010. The SMOS mission: new tool for monitoring key elements of the global water cycle. Proc. IEEE 98 (5), 666–687. <https://doi.org/10.1109/JPROC.2010.2043032>.
- Kerr, Y.H., Waldteufel, P., Richaume, P., Wigneron, J.P., Ferrazzoli, P., Mahmoodi, A., Al Bitar, A., Cabot, F., Gruhier, C., Juglea, S.E., et al., 2012. The smos soil moisture retrieval algorithm. IEEE Trans. Geosci. Rem. Sens. 50 (5), 1384–1403. <https://doi.org/10.1109/TGRS.2012.2184548>.
- Kerr, Y.H., Al-Yaari, A., Rodriguez-Fernandez, N., Parrens, M., Molero, B., Leroux, D., Bircher, S., Mahmoodi, A., Mialon, A., Richaume, P., et al., 2016. Overview of smos performance in terms of global soil moisture monitoring after six years in operation. Rem. Sens. Environ. 180, 40–63. <https://doi.org/10.1016/j.rse.2016.02.042>.
- Kerr, Y., Richaume, P., Waldteufel, P., Ferrazzoli, P., Wigneron, J., Schwank, M., Rautiainen, K., 2020. Algorithm Theoretical Basis Document (Atbd) for the Smos Level 2 Soil Moisture Processor. Technical Report TN-ESL-SM-GS-0001-4b SM-ESL (CBSA), p. 145p.
- Kim, H., Crow, W., Li, X., Wagner, W., Hahn, S., Lakshmi, V., 2023. True global error maps for smap, smos, and ascats soil moisture data based on machine learning and triple collocation analysis. Rem. Sens. Environ. 298, 113776 <https://doi.org/10.1016/j.rse.2023.113776>, 10.1016/j.rse.2023.113776.
- Koster, R.D., Dirmeyer, P.A., Guo, Z., Bonan, G., Chan, E., Cox, P., Gordon, C.T., Kanae, S., Kowalczyk, E., Lawrence, D., Liu, P., Lu, C.-H., Malyshev, S., McAvaney, B., Mitchell, K., Mocko, D., Oki, T., Oleson, K., Pitman, A., Sud, Y.C., Taylor, C.M., Verseghy, D., Vasic, R., Xue, Y., Yamada, T., 2004. Regions of strong coupling between soil moisture and precipitation. Science 305 (5687), 1138–1140. <https://doi.org/10.1126/science.1100217>.
- Larson, K., Small, E., Gutmann, E., Bilich, A., Braun, J., Zavorotny, V., Larson, C., 2008. Use of gps receivers as a soil moisture network for water cycle studies. Geophysical Research Letters - GEOPHYS RES LETT 35 (24). <https://doi.org/10.1029/2008GL036013>.
- Leavesley, A., 2010. Modelling Framework for Improved Agricultural Water-Supply Forecasting.
- Lebel, T., Cappelraere, B., Galle, S., Hanan, N., Kergoat, L., Levis, S., Vieux, B., Descroix, L., Gosset, M., Mougín, E., Peugeot, C., Seguis, L., 2009. AMMA-CATCH studies in the sahelian region of west-africa: an overview. J. Hydrol. 375 (1–2), 3–13. <https://doi.org/10.1016/j.jhydrol.2009.03.020>.
- Leroux, D., Kerr, Y.H., Richaume, P., Feiuzal, R., 2013. Spatial distribution and possible sources of SMOS errors at the global scale. Rem. Sens. Environ. 133, 240–250. <https://doi.org/10.1016/j.rse.2013.02.017>.
- Loew, A., Bell, W., Brocca, L., Bulgin, C.E., Burdanowitz, J., Calbet, X., Donner, R.V., Ghent, D., Gruber, A., Kaminski, T., et al., 2017. Validation practices for satellite based earth observation data across communities. Rev. Geophys. <https://doi.org/10.1002/2017RG000562>.
- Loveland, T., Zhu, Z., Ohlen, D., Brown, J., Redd, B., Yang, L., 1999. An analysis of igbp global land-cover characterization process. Photogramm. Eng. Rem. Sens. 65, 1069–1074.
- Marczewski, W., Slominski, J., Slominska, E., Usowicz, B., Usowicz, J., S, R., O, M., Nastula, J., Zawadzki, J., 2010. Strategies for validating and directions for employing smos data, in the cal-val project swex (3275) for wetlands. Hydrol. Earth Syst. Sci. Discuss. 7 (Sep) <https://doi.org/10.5194/hessd-7-7007-2010>.
- Mattar, C., Santamaría-Artigas, A., Durán-Alarcón, C., Olivera-Guerra, L., Fuster, R., Borvarán, D., 2016. The lab-net soil moisture network: application to thermal remote sensing and surface energy balance. Data 1 (1). <https://doi.org/10.3390/data1010006>.
- Matula, S., Bát'ková, K., Legese, W.L., 2016. Laboratory performance of five selected soil moisture sensors applying factory and own calibration equations for two soil media of different bulk density and salinity levels. Sensors 16 (11), 1912. <https://doi.org/10.3390/s16111912>.
- Mätzler, C., 1994. Microwave transmissivity of a forest canopy: experiments made with a beech. Rem. Sens. Environ. 48 (2), 172–180. [https://doi.org/10.1016/0034-4257\(94\)90139-2](https://doi.org/10.1016/0034-4257(94)90139-2).
- Merchant, C.J., Paul, F., Popp, T., Ablain, M., Bontemps, S., Defourny, P., Hollmann, R., Lavergne, T., Laeng, A., de Leeuw, G., Mittag, J., Poulsen, C., Povey, A.C., Reuter, M., Sathyendranath, S., Sandven, S., Sofieva, V.F., Wagner, W., 2017. Uncertainty information in climate data records from earth observation. Earth Syst. Sci. Data 9 (2), 511–527. <https://doi.org/10.5194/essd-9-511-2017>.
- Mialon, A., Coret, L., Kerr, Y.H., Sécherre, F., Wigneron, J.-P., 2008. Flagging the topographic impact on the smos signal. IEEE Trans. Geosci. Rem. Sens. 46 (3), 689–694. <https://doi.org/10.1109/TGRS.2007.914788>.
- Mironov, V., Bobrov, P., Fomin, S., 2013. Dielectric model of moist soils with varying clay content in the 0.04 to 26.5 ghz frequency range. In: 2013 International Siberian Conference on Control and Communications (SIBCON), pp. 1–4. IEEE.
- Moghaddam, M., Silva, A., Clewley, D., Akbar, R., Hussaini, S., Whitcomb, J., Devarakonda, R., Shrestha, R., Cook, R., Prakash, G., Santhana Vannan, S., Boyer, A., 2016. Soil moisture profiles and temperature data from soilscape sites, USA. <https://doi.org/10.3334/ORNLDAAAC/1339>.
- Molero, B., Leroux, D.J., Richaume, P., Kerr, Y.H., Merlin, O., Cosh, M.H., Bindlish, R., 2018. Multi-timescale analysis of the spatial representativeness of in situ soil moisture data within satellite footprints. J. Geophys. Res. Atmos. 123 (1), 3–21. <https://doi.org/10.1002/2017jd027478>.
- Morbiddelli, R., Corradini, C., Saltalippi, C., Flammini, A., Rossi, E., 2011. Infiltration-soil moisture redistribution under natural conditions: experimental evidence as a guideline for realizing simulation models. Hydrol. Earth Syst. Sci. 15 (9), 2937–2945.
- Muñoz-Sabater, J., De Rosnay, P., Albergel, C., Isaksen, L., 2018. Sensitivity of soil moisture analyses to contrasting background and observation error scenarios. Water 10 (7). <https://doi.org/10.3390/w10070890>.
- Ojo, E.R., Bullock, P., Heureux, J.L., Powers, J., McNairn, H., Pacheco, A., 2015. Calibration and evaluation of a frequency domain reflectometry sensor for real-time soil moisture monitoring. Vadose Zone J. 14 (3) <https://doi.org/10.2136/vzj2014.08.0114>.
- Osenga, E.C., Vano, J.A., Arnott, J.C., 2021. A community-supported weather and soil moisture monitoring database of the roaring fork catchment of the Colorado river headwaters. Hydrol. Process. 35 (3), e14081.
- Pan, L., Chen, Y., Xu, Y., Li, J., Lu, H., 2022. A model for soil moisture content prediction based on the change in ultrasonic velocity and bulk density of tillage soil under alternating drying and wetting conditions. Measurement 189, 110504. <https://doi.org/10.1016/j.measurement.2021.110504>.
- Pellarin, T., Mialon, A., Biron, R., Coulaud, C., Gibon, F., Kerr, Y., Lafaysse, M., Mercier, B., Morin, S., Redor, L., et al., 2016. Three years of l-band brightness

- temperature measurements in a mountainous area: topography, vegetation and snowmelt issues. *Rem. Sens. Environ.* 180, 85–98. <https://doi.org/10.1016/j.rse.2016.02.047>.
- Petropoulos, G.P., McCalmont, J.P., 2017. An operational in situ soil moisture & soil temperature monitoring network for west wales, UK: the wsmn network. *Sensors* 17 (7), 1481. <https://doi.org/10.3390/s17071481>.
- Phillips, T.J., Klein, S.A., Ma, H.-Y., Tang, Q., Xie, S., Williams, I.N., Santanello, J.A., Cook, D.R., Torn, M.S., 2017. Using ARM observations to evaluate climate model simulations of land-atmosphere coupling on the u.s. southern great plains. *J. Geophys. Res. Atmos.* 122 (21) <https://doi.org/10.1002/2017jd027141>.
- Poggio, L., de Sousa, L.M., Batjes, N.H., Heuvelink, G.B.M., Kempen, B., Ribeiro, E., Rossiter, D., 2021. Soilgrids 2.0: producing soil information for the globe with quantified spatial uncertainty. *SOIL* 7 (1), 217–240. <https://doi.org/10.5194/soil-7-217-2021>.
- Rasheed, M.W., Tang, J., Sarwar, A., Shah, S., Saddique, N., Khan, M.U., Imran Khan, M., Nawaz, S., Shamshiri, R.R., Aziz, M., Sultan, M., 2022. Soil moisture measuring techniques and factors affecting the moisture dynamics: a comprehensive review. *Sustainability* 14 (18), 11538. <https://doi.org/10.3390/su141811538>.
- Reid, I., Parkinson, R., 1984. The wetting and drying of a grazed and ungrazed clay soil. *J. Soil Sci.* 35 (4), 607–614. <https://doi.org/10.1111/j.1365-2389.1984.tb00618.x>.
- Rodriguez-Fernandez, N., Rixen, T., Boutin, J., 2024. The fine resolution explorer for salinity, carbon and Hydrology (FRESCH). A mission to study ocean-land-ice interfaces (submitted). In: *IGARSS 2024 - 2024 IEEE International Geoscience and Remote Sensing Symposium*.
- Sahr, K., White, D., Kimerling, A.J., 2003. Geodesic discrete global grid systems, *Cartography and Geographic. Inf. Sci.* 30 (2), 121–134. <https://doi.org/10.1559/152304003100011090>.
- Schaefer, G., Cosh, M., Jackson, T., 2007. The usda natural resources conservation service soil climate analysis network (scan). *Journal of Atmospheric and Oceanic Technology - J ATMOS OCEAN TECHNOL* 24 (12), 2073–2077. <https://doi.org/10.1175/2007JTECHA930.1>.
- Schlenz, F., dall'Amico, J.T., Loew, A., Mauser, W., 2012. Uncertainty assessment of the smos validation in the upper danube catchment. *IEEE Trans. Geosci. Rem. Sens.* 50 (5), 1517–1529.
- Schmugge, T., 1978. Remote sensing of surface soil moisture. *J. Appl. Meteorol.* 1962–1982, 1549–1557. <https://doi.org/10.1080/02626669609491523>.
- Seneviratne, S.I., Corti, T., Davin, E.L., Hirschi, M., Jaeger, E.B., Lehner, I., Orlowsky, B., Teuling, A.J., 2010. Investigating soil moisture–climate interactions in a changing climate: a review. *Earth Sci. Rev.* 99 (3), 125–161. <https://doi.org/10.1016/j.earscirev.2010.02.004>.
- Shin, D., Bellow, J., LaRow, T., Cocke, S., O'Brien, J.J., 2006. The role of an advanced land model in seasonal dynamical downscaling for crop model application. *J. Appl. Meteorol. Climatol.* 45 (5), 686–701. <https://doi.org/10.1175/JAM2366.1>.
- Smith, A., Walker, J., Western, A., Young, R., Ellett, K., Pipunic, R., Grayson, R., Siriwardena, L., Chiew, F., Richter, H., 2012. The murrumbidgee soil moisture monitoring network data set. *Water Resour. Res.* 48 (7) <https://doi.org/10.1029/2012WR011976>.
- Su, S.L., Singh, D., Baghini, M.S., 2014. A critical review of soil moisture measurement. *Measurement* 54, 92–105. <https://doi.org/10.1016/j.measurement.2014.04.007>.
- Tagesson, T., Fensholt, R., Guiro, I., Rasmussen, M.O., Huber, S., Mbow, C., García, M., Horion, S., Sandholt, I., Holm-Rasmussen, B., Göttsche, F.M., Ridler, M.-E., Olén, N., Olsen, J.L., Ehammer, A., Madsen, M., Olesen, F.S., Ardö, J., 2014. Ecosystem properties of semiarid savanna grassland in west africa and its relationship with environmental variability. *Global Change Biol.* 21 (1), 250–264. <https://doi.org/10.1111/gcb.12734>.
- Talone, M., Portabella, M., Martínez, J., González-Gambau, V., 2015. About the optimal grid for smos level 1c and level 2 products. *Geosci. Rem. Sens. Lett. IEEE* 12 (8), 1630–1634. <https://doi.org/10.1109/LGRS.2015.2416920>.
- Ulabay, F.T., Moore, R.K., Fung, A.K., 1981. *Microwave remote sensing active and passive*. In: *Microwave Remote Sensing Fundamentals and Radiometry*, Dedham, 1. Artech House, MA, USA.
- Van Cleve, K., Chapin, F., Ruess, R., 2015. *Bonanza Creek Long Term Ecological Research Project Climate Database*. university of alaska, fairbanks.
- van der Schalie, R., de Jeu, R., Kerr, Y., Wigneron, J., Rodríguez-Fernández, N., Al-Yaari, A., Parinussa, R., Mecklenburg, S., Drusch, M., 2017. The merging of radiative transfer based surface soil moisture data from smos and amsr-e. *Rem. Sens. Environ.* 189, 180–193. <https://doi.org/10.1016/j.rse.2016.11.026>.
- Wang, P., Zeng, J., Chen, K.-S., Ma, H., Zhang, X., Shi, P., Peng, C., Bi, H., 2024. Global-scale assessment of multiple recently developed/reprocessed remotely sensed soil moisture datasets. *IEEE Trans. Geosci. Rem. Sens.* 62, 1–18. <https://doi.org/10.1109/TGRS.2024.3361890>, 10.1109/tgrs.2024.3361890.
- Wigneron, J.-P., Kerr, Y.H., Waldteufel, P., Saleh, K., Escorihuela, M.-J., Richaume, P., Ferrazzoli, P., de Rosnay, P., Gurney, R., Calvet, J.-C., Grant, J.P., Guglielmetti, M., Hornbuckle, B., Mätzler, C., Pellarin, T., Schwank, M., 2007. L-band Microwave Emission of the Biosphere (L-MEB) Model : description and calibration against experimental data sets over crop fields. *Rem. Sens. Environ.* 107, 639–655. <https://doi.org/10.1016/j.rse.2006.10.014>.
- Xaver, A., Zappa, L., Rab, G., Pfeil, I., Vreugdenhil, M., Hemment, D., Dorigo, W.A., 2020. Evaluating the suitability of the consumer low-cost parrot flower power soil moisture sensor for scientific environmental applications. *Geoscientific Instrumentation, Methods and Data Systems* 9 (1), 117–139. <https://doi.org/10.5194/gi-9-117-2020>.
- Xu, X., Frey, S.K., 2021. Validation of smos, smap, and esa cci soil moisture over a humid region. *IEEE J. Sel. Top. Appl. Earth Obs. Rem. Sens.* 14, 10784–10793. <https://doi.org/10.1109/JSTARS.2021.3122068>.
- Yang, K., Qin, J., Zhao, L., Chen, Y., Tang, W., Han, M., Lazhu, Chen, Z., Lv, N., Ding, B., Wu, H., Lin, C., 2013. A multiscale soil moisture and freeze–thaw monitoring network on the third pole. *Bull. Am. Meteorol. Soc.* 94 (12), 1907–1916. <https://doi.org/10.1175/bams-d-12-00203.1>.
- Zreda, M., Shuttleworth, W.J., Zeng, X., Zweck, C., Desilets, D., Franz, T., Rosolem, R., 2012. COSMOS: the COsmic-ray soil moisture observing system. *Hydrol. Earth Syst. Sci.* 16 (11), 4079–4099. <https://doi.org/10.5194/hess-16-4079-2012>.